Available online at www.sciencedirect.com
ScienceDirect
International Journal of Heat and Mass Transfer 50 (2007) 5124–5138
International Journal of HEAT and MASS TRANSFER
www.elsevier.com/locate/ijhmt

Heat transfer characteristics of an impinging inverse diffusion flame jet. Part II: Impinging flame structure and impingement heat transfer

L.L. Dong [a,b,*], C.S. Cheung [b], C.W. Leung [b]

[a] Institute of Sustainable Energy Technology, School of the Built Environment, University of Nottingham, UK
[b] Department of Mechanical Engineering, The Hong Kong Polytechnic University, Hong Kong, China

Received 22 March 2007; received in revised form 25 June 2007
Available online 12 September 2007

Abstract

This paper is the second part of the experimental study on exploring the feasibility of inverse diffusion flame (IDF) for impingement heating. The structures and heat transfer characteristics of an impinging IDF jet have been studied. Four types of impinging flame structure have been identified and reported. The distributions of the wall static pressure are measured and presented. The influences of the global equivalence ratio (ϕ), the Reynolds number of the air jet (Re_{air}), and the non-dimensional burner-to-plate distance (H/d_{air}), on the flame structure, and the local and averaged heat transfer characteristics, are reported and discussed. The highest heat transfer occurs when the tip of the flame inner reaction zone impinges on the plate. The heat transfer rate from the impinging IDF is found to be higher than that in the premixed flame jet due to the augmented turbulence level originated from the flame neck. This high heat transfer rate, together with its in-born advantage of no danger of flashback and low level of nitrogen oxides emission, demonstrates the blue, dual-structured, triple-layered IDF is a desirable alternative for impingement heating.
© 2007 Elsevier Ltd. All rights reserved.

Keywords: Flame impingement; Inverse diffusion flame; Heat transfer enhancement; Flame structure

1. Introduction

Flame impingement heating has been widely used in domestic and industrial applications due to the high localized convective heat transfer rate. Lot of studies have been carried out to understand the full picture of the characteristics of the flame impingement system, ranging from the flow and flame structure [1–5], the heat transfer characteristics [6–11], to the pollutants emission characteristics [12–15]. Premixed or partially premixed flame has been chosen as the impinging flame in most previous investigations due to the high flame temperature and less or no soot emission [16–21]. On the other hand, premixed or partially premixed flame has safety and stability concerns because of the possibility of flashback and liability to blow off. In an attempt to address these concerns, the present investigation is motivated to explore the feasibility of the inverse diffusion flame (IDF) for impingement heating, as an alternative alongside with premixed or partially premixed flame jets. The first part of this investigation has dealt with the flame structures of the free IDF. It is found that the blue dual-structured, triple-layered IDF has a premixed flame structure in the torch flame beyond the flame neck. The flame neck acts as a mixer of the fuel and air, and it anchors the premixed torch flame beyond it. This unique flame structure provides the IDF with good self-stabilizing capability. The IDF is able to maintain stable until Re_{air} reaches 8000. In comparison, the premixed flame or partially premixed flame normally cannot stabilize without external help when the flame becomes turbulent when Reynolds number exceeds 2000. This premixed flame structure, good self-stabilizing capability, together with the inborn characteristics of no danger of flashback, makes the IDF

* Corresponding author. Address: Institute of Sustainable Energy Technology, School of the Built Environment, University of Nottingham, UK.
E-mail address: leilei.dong@nottingham.ac.uk (L.L. Dong).

0017-9310/$ - see front matter © 2007 Elsevier Ltd. All rights reserved.
doi:10.1016/j.ijheatmasstransfer.2007.07.017

Nomenclature

d	diameter (m)
H	distance between the nozzle and the impingement plate (m)
P	static wall pressure (Pa)
$\dot{q}$	heat flux density (W/m^2)
r	radial distance from stagnation point (m)
Re	Reynolds number ($= u_{air}d_{air}/v_{air}$)
T	temperature (K)
u	gas velocity (m/s)

Greek symbols

v	kinematic viscosity (m^2/s)
Φ	equivalence ratio (= (stoichiometric air/fuel volume ratio)/(actual air/fuel volume ratio))

Superscript

–	averaged value

Subscripts

air	air jet
f	flame jet
max	maximum value
p	impingement plate
s	the stagnation point

a desirable option for impingement heating. This paper is the second part of the investigation on exploring the feasibility of impinging IDF for impingement heating. The local and averaged heat transfer characteristics of the impinging IDF have been studied and reported. The influences of ϕ, Re_{air}, and H/d_{air} on the impinging flame structure and impingement heat transfer have been discussed.

2. Experimental setup and methods

The Experimental setup is shown schematically in Fig. 1. The details of the IDF burner has been introduced in the first part of this paper and will not be repeated. In this part, the additional experimental setup, i.e., the heat absorption system, will be introduced. The flame impingement surface is a rectangular copper plate of 200 mm long, 200 mm wide and 8 mm thick. It is evenly cooled on the backside by a cooling water jacket. Copper was selected because of its excellent thermal conductivity. The top plate of the cooling water jacket is made of plexiglass to enable the water flow visible. After any change in the operating condition, measurements are only made after the steady-state condition had been established again and the exit temperature of the cooling water has been stabilized. The local heat flux from the flame to the plate is measured with a coated Vatell HFM-6 microsensor installed inside the impingement plate. The sensor surface is flush with the front side of the plate facing the flame. The output voltage signal is recorded by a stand-alone IOtech data acquisitor after being amplified by an AMP-6 amplifier. The radial heat flux distribution is obtained with 1 mm apart by moving the burner positioner horizontally. A single pressure tap of 1 mm diameter was drilled through the copper plate at its center. The radial pressure distributions along the plate are obtained by moving the three-dimensional burner positioner in the x-, y- and z-directions, while the plate remained stationary. The pressure tap is connected via a flexible tube to an inclined differential manometer with an accuracy of ±2% of the full scale. Direct images of the flames are obtained with a digital camera.

Experiments are designed and carried out to study the flame structure and heat transfer characteristics of the impinging IDFs under the respective influences of Re_{air}, H/d_{air} and ϕ. Re_{air} is selected to range from 3000 to 8000, where a dual-structure triple-layer IDF is formed with or without yellow soot neck. H/d_{air} stretches from 1.5 to 16.5 covering different impinging flame structures from potential core impingement to post-flame impingement. ϕ is chosen extending from fuel-lean condition

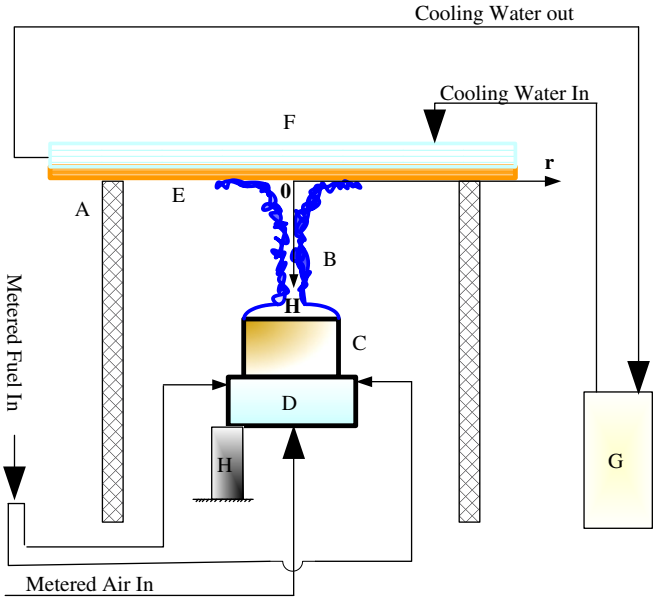

A: Screen Mesh **B: Inverse Diffusion Flame**
C: Burner Head **D: Settling Chamber**
E: Brass Impingement Plate **F: Cooling Water Jacket**
G: Thermalstat **H: 3-D Positioner**

Fig. 1. Schematic of the IDF impingement setup.

($\Phi = 0.8$) to fuel-rich condition ($\Phi = 2.1$). Both local and averaged heat fluxes are measured and reported.

The experimental uncertainty analysis is performed with the method of Kline and McClintock [22]. With 95% confidence level, the minimum and maximum uncertainties in the flame temperature measurements are 2.6% and 10.4%, respectively. The uncertainty of the heat flux measurement ranges between 1.1% and 8.2%, respectively. The minimum and maximum uncertainties of CO measurement are 2.1% and 9.5%, respectively. The uncertainty of the NO measurement covers from 2.3% to 12.3%, respectively. The minimum uncertainties of CO_2 and O_2 are 1.1% and 1.3%, respectively, while their maximum uncertainties are 8.3% and 9.2%, respectively.

3. Shape and structure of an impinging IDF

For a given configuration of flame impingement system, it has been found the characteristics of the system is mainly dependent of the global equivalence ratio, ϕ, the non-dimensional nozzle-to-plate distance, H/d_{air}, and the discharging velocity of the air jet, Re_{air}. Therefore, the present experimental study concentrates on the influences of these three factors on the flame structures and heat transfer characteristics of the impinging IDF, which will be discussed in detail in the following.

The direct flame photos under different H/d_{air}, ϕ, and Re_{air} are shown from Figs. 2–4, respectively. It is observed from Fig. 2 that under smaller H/d_{air} of 3, both the inner reaction cone and the outer diffusion flame impinge on the plate, with a perceptible circular hole in the center. This circular central hole is found to be very cool and composed of the unreacted gas mixture. Both the inner reaction zone and the outer diffusion flame spread outwards radially along the plate after impingement, forming wall jet flame. It is found from Fig. 2a that the IDF covering the plate is characterized by three concentric circles. They are formed respectively by the unreacted gas in the center, the reaction zone in the middle, and the diffusion layer in the outmost. It is reasonable to predict that the sharp variation of the T_{f} in these three rings results in a considerably non-uniform distribution of heat flux along the plate. When increasing the H/d_{air}, the radius of these flame rings all decrease accordingly, as shown in Fig. 2b. When the H/d_{air} is large enough, the inner cone tip just impinges on the plate. When further increasing H/d_{air}, it is the outer diffusion flame that impinges on the plate, forming a circular flame adjacent to the plate, with no flame rings covering the plate any more, as shown in Fig. 2c.

The influence of the ϕ on the flame shape is shown in Fig. 3. It is observed that under fuel-lean condition, i.e., $\Phi = 0.8$, the tip of the inner reaction zone is truncated with no perceptible outer diffusion layer. This is because the fuel has been consumed along the way before forming the tip. When ϕ is increased to 1.0, a closed reaction zone starts to appear. It can also be observed that as increasing ϕ, the inner reaction cone becomes longer and thicker, with

(a) $H/d_{air} = 3$

(b) $H/d_{air} = 6$

(c) $H/d_{air} = 11$

Fig. 2. Photos of impinging IDF under $Re_{\text{air}} = 8000$, $\Phi = 1.8$.

increasing in the length of the inner cone tip as well. The area of the plate covered by the impinging flame is also increased with increasing the ϕ due to the prolonged flame length.

The flame shapes under different Re_{air} is shown in Fig. 4. When $Re_{\text{air}} = 3000$, the flame is yellow in the flame neck and part of the flame tip, indicating soot formation due to incomplete fuel/air mixing. In this case, the velocity of the air jet is not large enough to create stronger suction to produce deeper penetration length of the impinging fuel jets. Thus, the fuel/air mixing in the flame neck is insufficient, leading to a fuel-rich zone in the fuel side of the flame neck. Therefore, a yellow outer soot ring is formed. The soot emission in the top diffusion layer also indicates the fuel-rich condition in this region. As increasing the Re_{air} to 4000, the flame above the neck is blue. Only a much weakened soot ring is still there in the flame neck, indicating the enhanced fuel/air mixing in the flame neck and

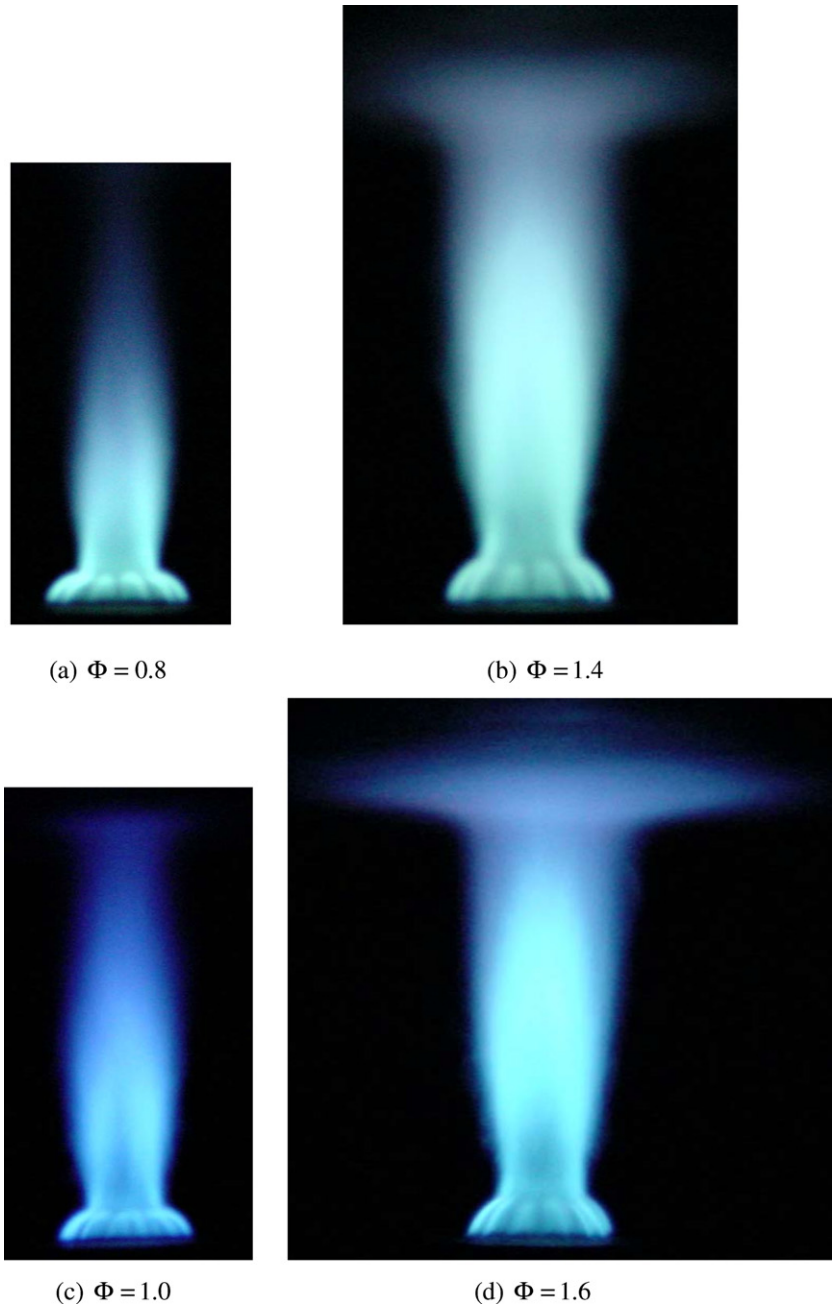

Fig. 3. Photos of IDF under $Re_{air} = 8000$, $H/d_{air} = 11$.

beyond. When further increasing the Re_{air} to 5000, it is observed that the yellow neck soot ring disappears completely and the flame becomes all blue. On the other hand, it is also observed that the lengths of the inner reaction zone and the outer diffusion layer increase with increasing Re_{air}, with the inner cone tip closer to the impingement plate and more area of the plate covered by the deflected flame. The inner cone also becomes thicker and the inner cone tip becomes longer as increasing Re_{air} due to increased turbulence.

In summary, four types of impinging IDF have been identified corresponding to the different part of the flame impinging on the plate in the stagnation point. These are impingement of the open inner reaction zone, which is formed with or without the influence of the plate, the impingement of the tip of the inner reaction zone and the impingement of the post-flame zone. These four flame structures are shown schematically in Fig. 5. It is shown in Fig. 5 that the mixing of the fuel and air is mainly caused by the suction, together with entrainment of the surrounding air. Fig. 5a represents the structure of the IDF under small H/d_{air} where the inner cone is forced to open due to the plate, as shown previously in Fig. 2a and b. Fig. 5b and c represents the flame structures with impingement of inner cone tip and post-flame zone, respectively. Fig. 5d represents the flame under fuel-lean condition

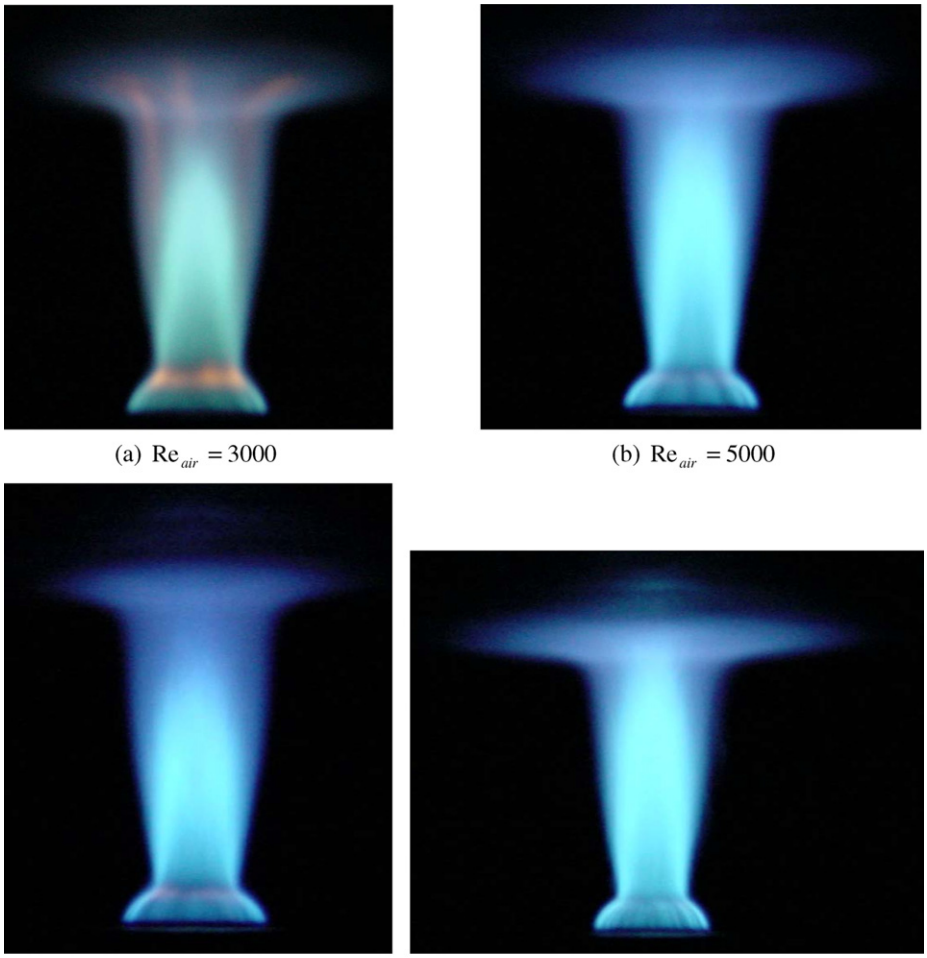

Fig. 4. Photos of IDF under $\Phi = 1.4$, $H/d_{air} = 9$.

where the inner cone is open before the impingement, as shown in Fig. 3a. Different flame structure results in different heat transfer performance, as to be discussed in the following.

4. Wall pressure distribution

The static wall pressure distribution is closely related to the hydrodynamic characteristics of the impinging IDF. Here we put the emphasis on the stagnation point static pressure because it is the location where the velocity is fully arrested. The effects of H/d_{air} and ϕ on the wall static pressure distributions are discussed, respectively.

4.1. Effects of H/d_{air}

The variations of the wall static pressure distributions under different H/d_{air} are shown in Fig. 6. The H/d_{air} varies from a very low level of 1.5 to a high value of 16.5, resulting in different pressure distribution patterns. The discussion is presented on two separate regions, i.e., the region around the stagnation point of $-1.0 < r/d_{air} < 1.0$, where the pressure gradient is very large, and the region beyond it where the pressure variation is rather flat. It is observed that in the region of $-1.0 < r/d_{air} < 1.0$, the pressure distributions under $H/d_{air} = 1.5$ and $H/d_{air} = 3$ are very similar in shape and quantity. The pressure at the stagnation point is as high as 380 Pa. Then it decreases sharply to below 60 Pa at around $r/d_{air} = 1.0$. The rapid decrease in the wall pressure indicates the fast acceleration in the radial spreading velocity. The similar pressure level at the stagnation point in these two cases suggests the similar velocity when impinging on the plate. This indicates that it is the flow in the potential core that directly impinges on the plate under these two conditions, because in the potential core region, the flow velocity is kept constant as the jet exit velocity. When the H/d_{air} increases to 4.5, the stagnation point pressure decreases dramatically due to the declining in the impinging velocity. Thus, we can conclude the potential core length of the impinging IDF is located between $3.0d_{air}$ and $4.5d_{air}$. The stagnation point pressure decreases gradually with increase in H/d_{air} until $H/d_{air} = 13.5$, where the pressure level is very low of around 10 Pa. When H/d_{air} is further increased to 16.5, only slight decrease in stagnation

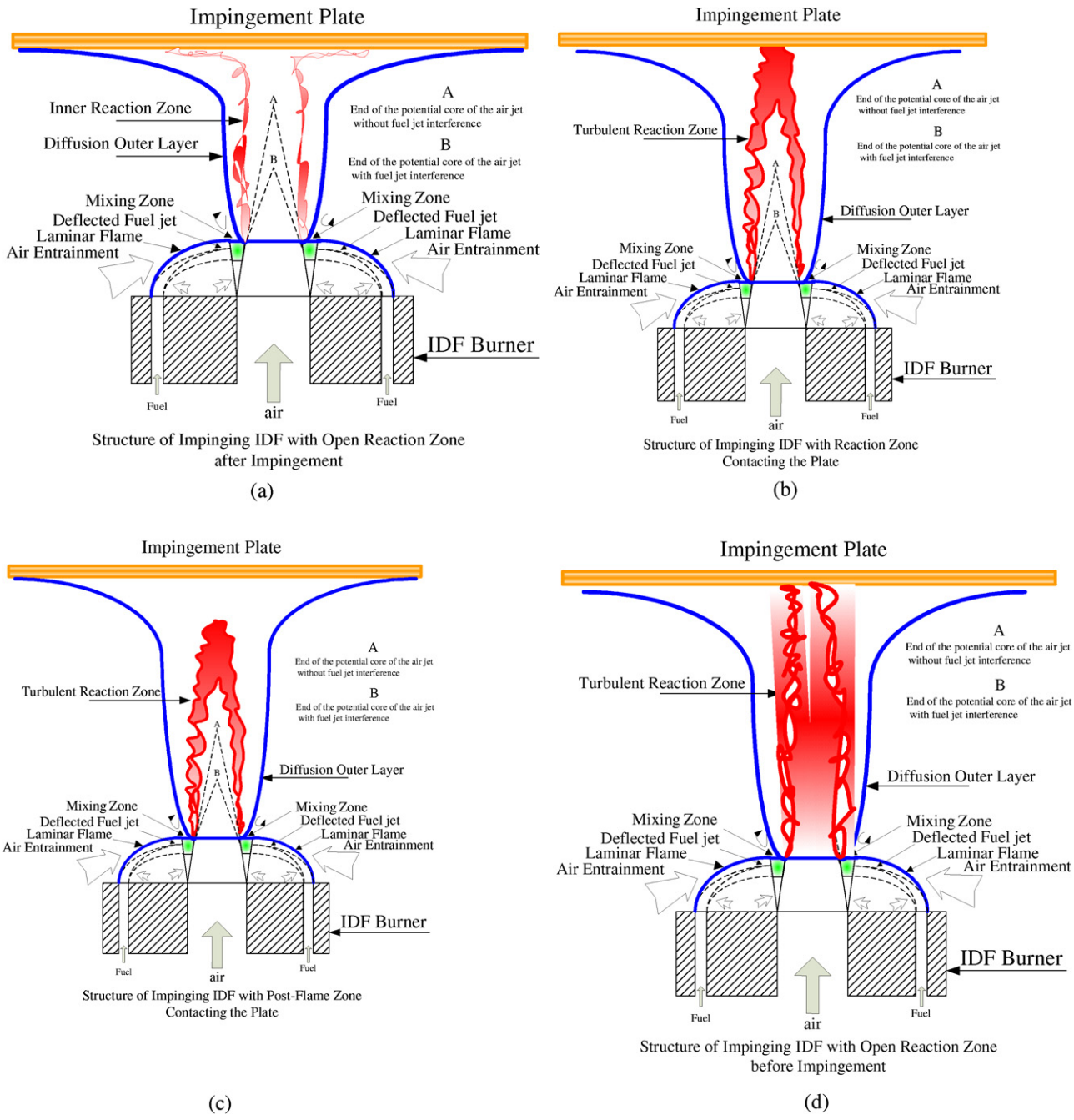

Fig. 5. Mapping of the structures of impinging IDFs.

point is observed. This low level of P_s when $H/d_{air} > 13.5$ corresponds to the low level of impinging velocity due to the longer traveling distance of the IDF before impinging on the plate. The low level of velocity indicates that the effect of the jet exiting velocity on the heat transfer at the stagnation point could be too small to be neglected. It is also observed from Fig. 6 that the pressure gradient at the stagnation point is considerably large under small H/d_{air} below 3.0. After that, the pressure gradient decreases gradually with increase in the H/d_{air} until $H/d_{air} = 7.5$, where the gradient at the stagnation point disappears. Instead, a pressure plateau appears in the region of $-0.6 < r/d_{air} < 0.6$. This variation of the pressure distribution pattern is due to the different flame structure. It is observed that, when $H/d_{air} < 7.5$, the cool gas inside the inner reaction zone impinges on the plate around the stagnation point. Under $H/d_{air} = 7.5$, the inner cone tip just reaches the plate. The chemical reaction occurs in the region of $-0.6 < r/d_{air} < 0.6$, where the intense heat release decreases the flame gas density. This density reduction offsets the flow acceleration in the radial direction in this region, and thus keeps the static pressure constant according to the Bernoulli's equation. When further increasing H/d_{air} to a height where the post-flame zone impinges on

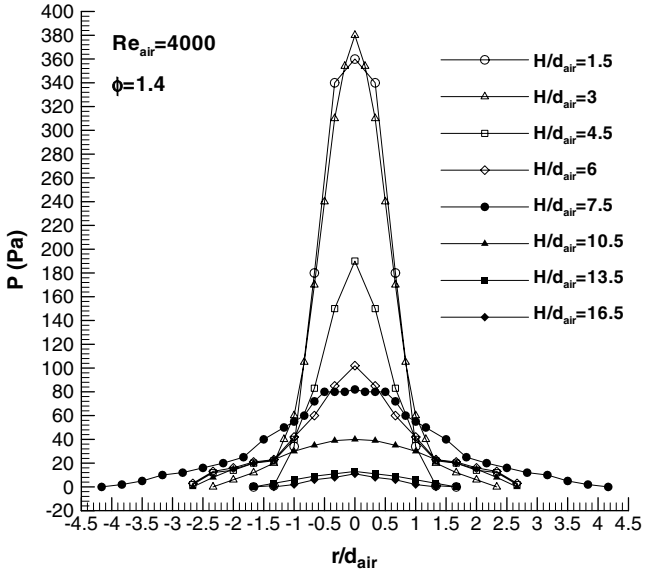

Fig. 6. Variations of the static pressure with H/d_{air}.

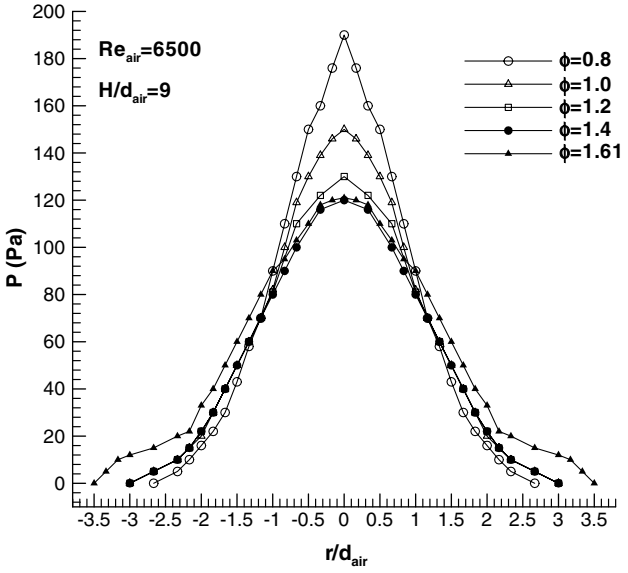

Fig. 7. Variations of the static pressure with Φ.

the plate, the gradual decrease in the wall pressure from the stagnation point is observed again, as shown in Fig. 6 due to the difference in the flame temperature and density in the radial direction.

When $r/d_{air} > 1.0$, the wall pressure continues to decrease at different paces under $H/d_{air} < 7.5$ until r/d_{air} reaches around 1.3. After that, the wall pressure decreases with decreasing in the H/d_{air}. This smaller wall pressure under smaller H/d_{air} indicates a larger radial velocity. This increase in wall pressure with increasing H/d_{air} in not found when $H/d_{air} > 7.5$ when the post-flame zone impinges on the stagnation point. Conversely, the wall pressure starts to decrease with increasing H/d_{air}. This is due to the decrease in the stagnation point wall pressure with increasing H/d_{air}. It can also be observed from Fig. 6 that the length of the impingement region, which extends from the stagnation point to where the wall pressure becomes zero, firstly increases from $r/d_{air} = 1.8$ to $r/d_{air} = 4.2$ with increasing H/d_{air} from 1.5 to 7.5. Then it decreases to $r/d_{air} = 1.7$ with further increasing in H/d_{air} to 16.5.

4.2. Effects of the ϕ

The influence of the ϕ on the static wall pressure distribution under $Re_{air} = 6500$ and $H/d_{air} = 9$ is shown in Fig. 7. It is observed that under $\Phi = 1.4$ and $\Phi = 1.61$, the tip of the inner reaction zone just impinges on the plate. It is found from Fig. 7 that in the region near the stagnation point of $-0.6 < r/d_{air} < 0.6$, the wall pressure decreases with increasing ϕ from 0.8 to 1.4. The pressure gradient becomes smaller with increasing ϕ. The decrease in the P_s indicates the decreasing impinging velocity, i.e., the air jet exit velocity decreases faster under the larger ϕ given the same traveling distance, i.e., the H/d_{air}. This is because more fuel is sucked and impinges on the air jet under larger ϕ, which thus reduces the air jet velocity because more dynamic energy is dissipated by mixing with the fuel jets. The pressure gradient comes larger with smaller ϕ, indicating a faster acceleration of the radial flow after impingement. When the ϕ further increases from 1.4 to 1.61, the wall pressure in the region is in the similar level. When the r/d_{air} is greater than 1.0, it is observed that the pressure comes lowest under $\Phi = 0.8$. The difference in the wall pressure is unidentifiable when increasing ϕ from 1.0 to 1.4. Although the difference in wall pressure in the region around the stagnation point is very small between $\Phi = 1.4$ and $\Phi = 1.61$, the wall pressure comes larger under $\Phi = 1.61$ than that under $\Phi = 1.4$ in the other regions. It is found that the impingement region increases generally with increase in ϕ ranging from $r/d_{air} = 2.7$ under $\Phi = 0.8$ to $r/d_{air} = 3.5$ under $\Phi = 1.61$.

5. Local heat transfer characteristics

The radial heat flux distributions under different H/d_{air}, ϕ and Re_{air} are discussed respectively. The emphasis is put on the variations of the stagnation point heat flux, the maximum heat flux, and the distributions in the impingement region and the wall jet region, respectively.

5.1. Effects of H/d_{air}

The heat flux distributions under a wide range of H/d_{air} from 1.5 to 16.5 are presented in Fig. 8. The measurements are carried out under four Re_{air} of 3000, 4000, 5000 and 8000, respectively. The ϕ is selected to be 1.4 in all the four cases because it is found to be able to produce the highest levels of local and average heat fluxes.

It is found from Fig. 8a that the heat flux varies differently under different H/d_{air}. Generally, two heat flux distri-

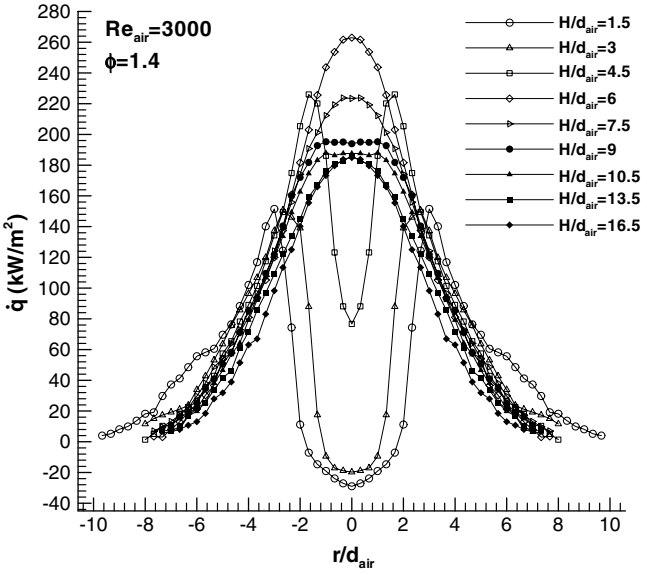

Fig. 8a. Variations of heat flux with H/d_{air} under $Re_{air} = 3000$.

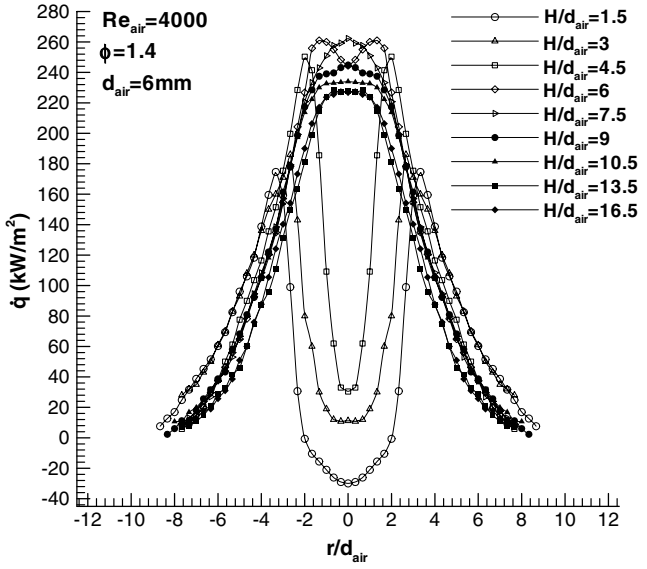

Fig. 8b. Variations of heat flux with H/d_{air} under $Re_{air} = 4000$.

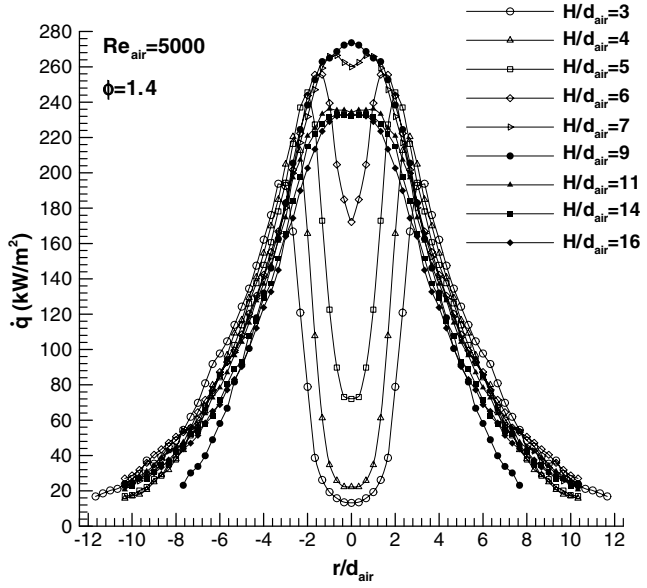

Fig. 8c. Variations of heat flux with H/d_{air} under $Re_{air} = 5000$.

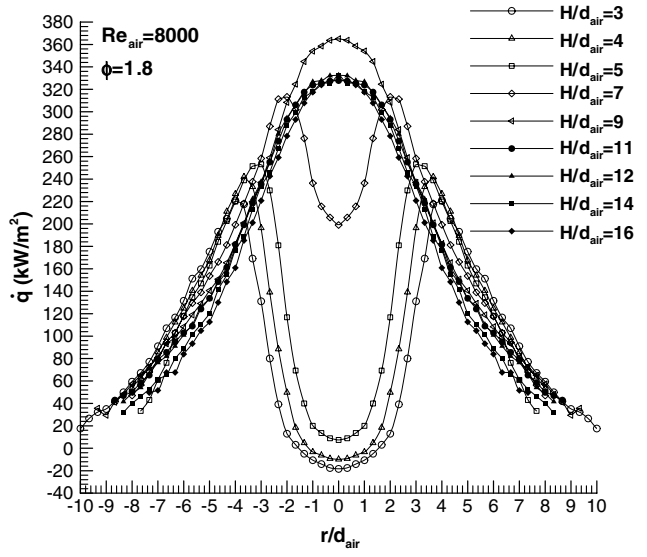

Fig. 8d. Variations of heat flux with H/d_{air} under $Re_{air} = 8000$.

bution patterns are found. When H/d_{air} is lower than 6, a cool central core of low heat flux region is found, with the heat flux at the stagnation point being the lowest and the maximum heat flux shifted some distance away. Thus the heat flux distribution is featured with two maximum heat flux points and one minimum heat flux point. When H/d_{air} reaches 6 and beyond, the heat flux generally varies following a bell-shaped curve, with the stagnation point heat flux being the peak value.

When H/d_{air} is lower than 6, it is found from Fig. 8a that the $\dot{q}_s$ increases with increasing H/d_{air}. This is due to the increased temperature of the flame that contacts the plate. It is also observed that $\dot{q}_s$ is negative when H/d_{air} is lower than 3.0, indicating an adverse heat transfer form plate to the flame. This is due to the direct impingement of the cold unreacted gas with the temperature lower than that of the plate. The stagnation point heat flux reaches the peak value when H/d_{air} is increased to 6.0 where the inner cone tip just impinges on the plate. Then the $\dot{q}_s$ decreases gradually when further increasing H/d_{air} to 10.5. The $\dot{q}_s$ remains almost unchanged when H/d_{air} is further increased to 16.5. Under the current experimental conditions, there are three factors that could possibly affect the heat transfer from the flame to the plate, i.e., the T_f, the impinging velocity and the heat release from chemical reaction. The measurements show that the T_f remains a constant high level from the reaction zone to the post-flame zone at $H/d_{air} = 20$. Therefore, the influence of T_f can be negligible

in the present conditions. Note that when H/d_{air} is larger than 6, it is the post-flame zone that impinges on the plate, although there is still exothermic reaction being taking place, like the complete oxidation of CO to CO_2, the heat release rate is far less than that in the inner reaction zone. Thus, the augmentation of heat release in heat transfer can be reasonably neglected. As a result, in the range of $H/d_{air} > 6$, only one major factor is left affecting the heat transfer rate, i.e., the impinging velocity. The enhancement of $\dot{q}_s$ under $H/d_{air} = 6$ is contributed by two factors, i.e., the extra heat released from the reaction and the high level of impinging velocity or the convective heat transfer coefficient. We have already known that the P_s decreases monotonically in the post-flame impingement conditions. This suggests a steadily decrease in the impinging velocity, which lowers the convective heat transfer coefficient and thus the heat transfer rate. When H/d_{air} is exceeding around 11, the P_s becomes very small. These are the conditions where the influence of the air jet velocity is almost unfelt. Thus, the heat transfer rate is only dependent of the flame temperature. Therefore, the $\dot{q}_s$ under $H/d_{air} = 13.5$ and $H/d_{air} = 16.5$ are the same, as shown in Fig. 8a.

It is also observed from Fig. 8a that maximum heat flux also increases with increase in the H/d_{air} till the maximum value achieved under $H/d_{air} = 6.0$. The location of the maximum heat flux lies further away from the stagnation point when decreasing H/d_{air} from 6.0 to 1.5. The maximum heat flux occurs where the flame temperature is high with occurrence of chemical reaction. The further the location of the maximum heat flux, the larger the cool central heat flux core. The radial flow is accelerated more rapidly under small H/d_{air}, as discussed with Fig. 9, which pushes the location of the reaction zone, or the maximum heat flux, further away.

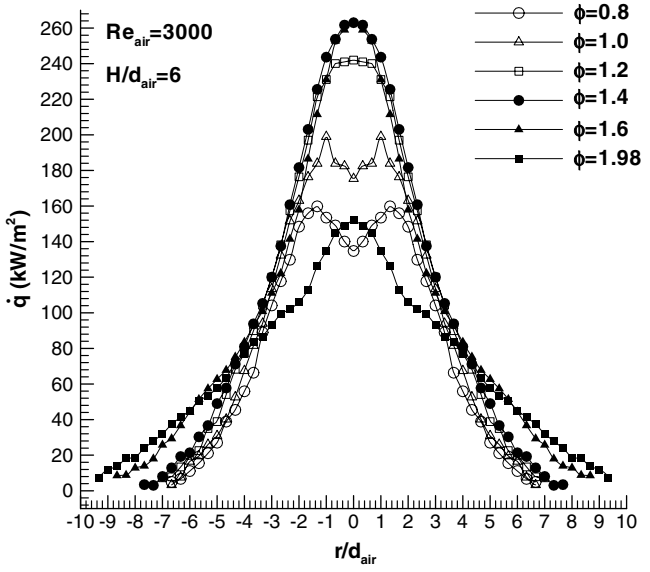

Fig. 9a. Variations of heat flux with Φ under $Re_{air} = 3000$, $H/d_{air} = 6$.

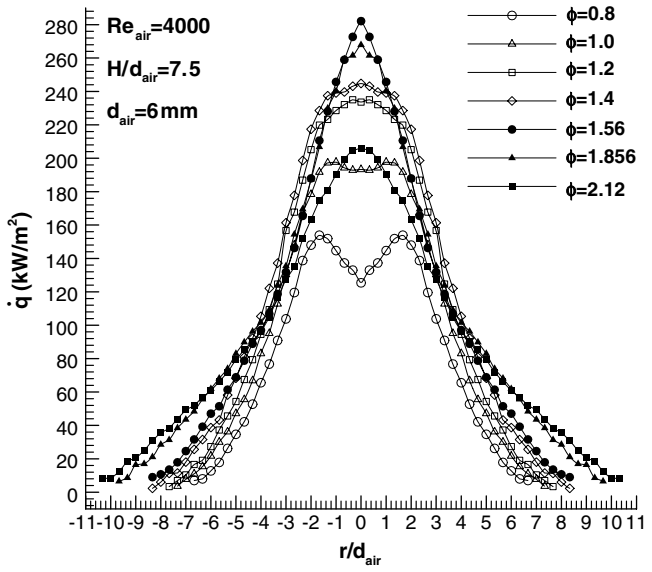

Fig. 9b. Variations of heat flux with Φ under $Re_{air} = 4000$, $H/d_{air} = 7.5$.

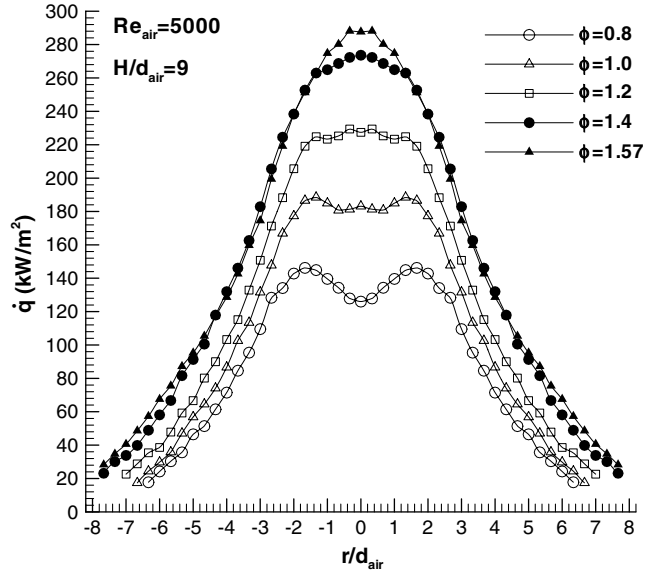

Fig. 9c. Variations of heat flux with Φ under $Re_{air} = 5000$, $H/d_{air} = 9$.

It is found from Fig. 8a that in the area of $r/d_{air} < 2.0$, which is approximately the impingement zone, the local heat flux first increases monotonically with increasing H/d_{air} till $H/d_{air} = 6.0$. Then the heat flux decreases gradually with further increase in H/d_{air} till $H/d_{air} = 13.5$. Beyond this, no clear decrease in heat flux is found when H/d_{air} is further increased to 16.5. This variation trend is similar to that of stagnation point heat flux, as discussed in the above. The local heat fluxes under different H/d_{air} continues to decrease when $r/d_{air} > 2.0$, following each trend line which is evidently intertwined until $r/d_{air} = 3.0$. Beyond that, the difference in the local heat flux under different H/d_{air} is not that large as in the impingement zone. In general, the heat flux increases slightly with the decrease

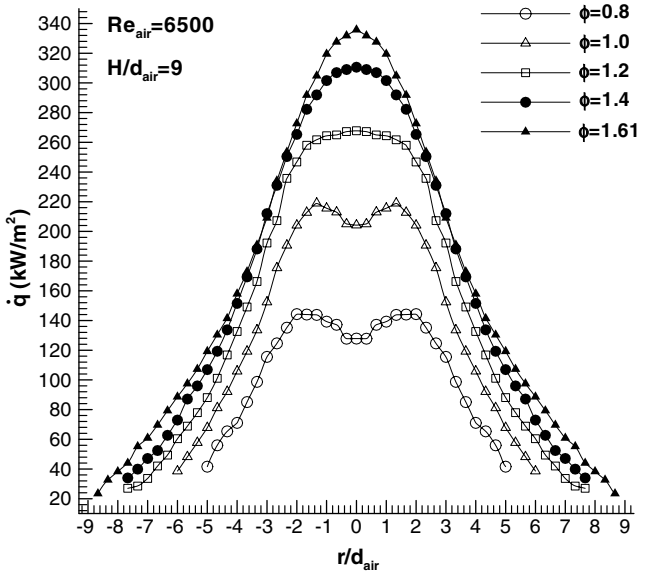

Fig. 9d. Variations of heat flux with Φ under $Re_{air} = 6500$, $H/d_{air} = 9$.

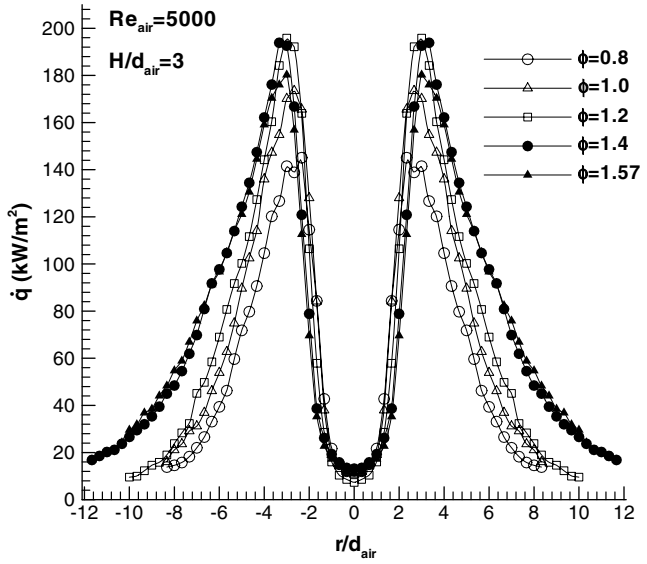

Fig. 9f. Variations of heat flux with Φ under $Re_{air} = 5000$, $H/d_{air} = 3$.

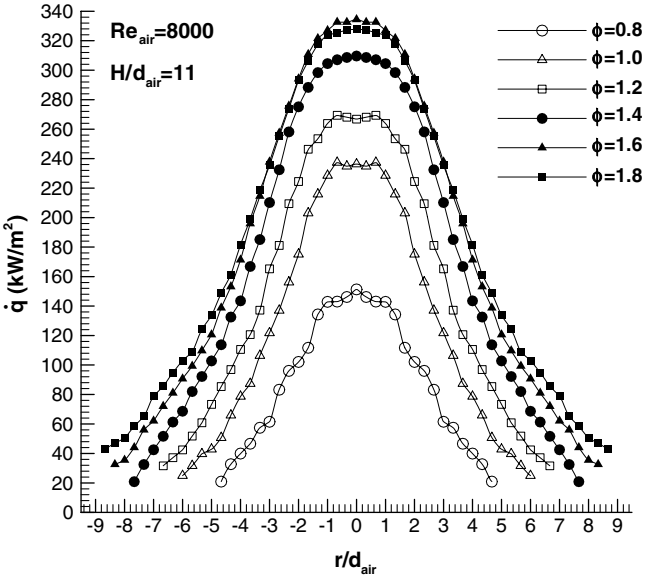

Fig. 9e. Variations of heat flux with Φ under $Re_{air} = 8000$, $H/d_{air} = 11$.

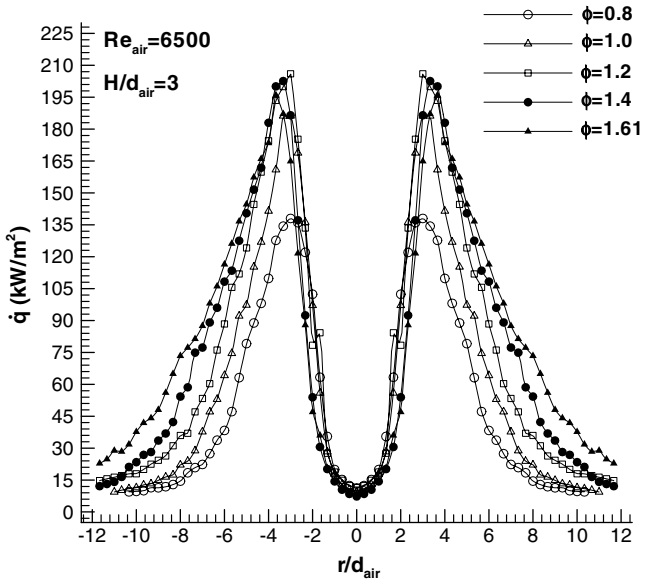

Fig. 9g. Variations of heat flux with Φ under $Re_{air} = 6500$, $H/d_{air} = 3$.

in H/d_{air}, although this slight increase cannot be clearly identified in some cases.

The variations of the local heat flux with H/d_{air} under Re_{air} of 4000 and 5000 with $\Phi = 1.4$, are shown in Figs. 8b and 8c, respectively. Fig. 8d presents the variations under higher ϕ of 1.8 and Re_{air} of 8000. It can be observed that the distribution characteristics is similar to that discussed under $Re_{air} = 3000$. Under all these three conditions, the heat flux distribution is characterized with the cool central core when the unreacted gas inside the inner reaction cone impinges directly on the plate. The stagnation point heat flux and the maximum heat flux increase firstly with the increase in H/d_{air} till when the tip of the inner reaction zone impinges on the plate. Then they decrease with further increase in the H/d_{air}, until a constant level is achieved under larger H/d_{air} of above 11. The value of the H/d_{air} where the maximum heat flux is reached is 7.5, 9, and 9, respectively corresponding to each Re_{air} of 4000, 5000 and 8000. By comparing Fig. 8d to the other three pictures, it is observed that under larger ϕ of 1.8, the heat flux decreases more slowly than that under smaller ϕ of 1.4, especially in the wall jet region due to longer flame length.

5.2. Effects of the ϕ

The variations of the heat flux distribution with ϕ under different H/d_{air} and Re_{air} are shown in Figs. 9a and 9h, respectively. The local heat flux distributions under H/d_{air}

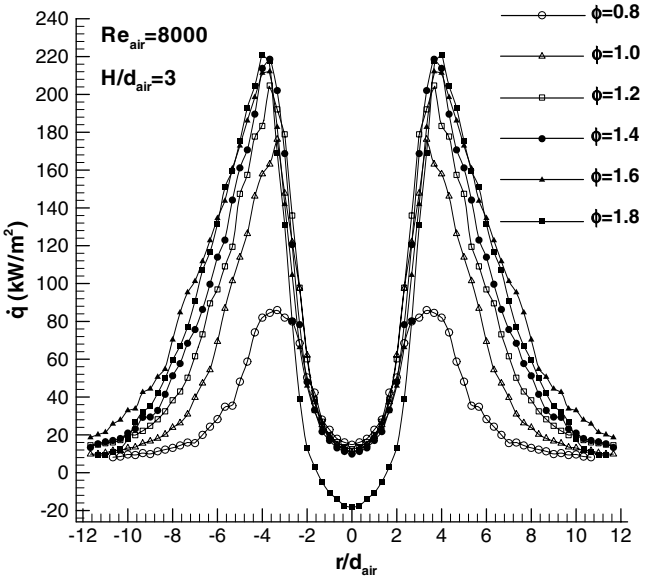

Fig. 9h. Variations of heat flux with Φ under $Re_{air} = 8000$, $H/d_{air} = 3$.

where the tip of the inner reaction zone impinges on the plate, are presented from Figs. 9a–9d under Re_{air} of 3000, 4000, 5000 and 6500, respectively. The heat flux variation trend when the post-flame zone impinges on the plate is shown in Fig. 9e, while the heat flux distributions under smaller H/d_{air} of 3.0 when the cold unreacted gas inside the inner reaction cone impinges on the plate, are shown from Figs. 9f–9h, respectively. ϕ is selected to range from fuel-lean condition when $\Phi = 0.8$ to fuel-rich condition when $\Phi = 2.12$, covering blue IDF and the IDF with yellow tip and neck.

It is observed from Fig. 9a that when $\Phi < 1.2$, the heat flux variation trend line is featured with two apexes located away from the stagnation point with the stagnation point heat flux coming lowest between them. The coincidence of the maximum heat flux point and the stagnation point starts to occur when $\Phi \geqslant 1.4$. The location of the maximum heat flux corresponds to the position where chemical reaction occurs. This is the result of the impingement of an open-tip IDF. When $\Phi \leqslant 1.0$, the IDF is found to be open in the tip before impingement, leaving the reaction layer away from the stagnation point. According to the measurement, the reaction cone tip in the free IDF in the same experimental condition is only visibly open under fuel-lean condition of $\Phi \leqslant 0.25$. This occurrence of the tip-openness under the larger ϕ in the impinging flame is due to the quenching effect of the cold plate. When ϕ reaches to 1.2, a high heat flux plateau is observed around the stagnation point. The difference of the heat flux between each location is in the error range. The stagnation point heat flux under $\Phi = 1.4$ is found to be similar to that under $\Phi = 1.6$. This is because they have the same flame structure, i.e., it is the reaction cone tip that impinges on the plate under these two conditions. It is found that the IDF is generally blue when $\Phi \leqslant 1.6$. When ϕ is further increased to 1.98, soot emission is observed on the tip of the flame, indicating incomplete combustion due to excess fuel provision. This yellow flame impingement gives rise to a significant decrease in the maximum/stagnation point heat flux.

It is also observed from Fig. 9a that the maximum heat flux also increases with increase in ϕ until $\Phi = 1.4$. For the tip-open impinging IDF, the location of the maximum heat flux shifted outwards when decreasing the ϕ. This is because more section of the inner reaction cone tip is truncated under lower ϕ. It is measured that the flame temperature decreases with decreasing ϕ when $\Phi \leqslant 1.2$. The lowered flame temperature makes the reaction cone tip to be easier to be quenched by the plate, resulting in a larger central hole inside the reaction layer. Thus, the maximum heat flux is located further away under smaller ϕ.

From Fig. 9a we can also observe that for the blue IDF when $\Phi < 1.6$, the local heat flux increases monotonically with increase in the ϕ. Generally, yellow-tip IDF produces reduced heat flux in the impingement region and enhanced heat flux in the wall jet region.

The similar heat flux variation trend is also found under Re_{air} of 4000, 5000, and 6500, as shown from Figs. 9b–9d, respectively. It is observed that the maximum heat flux occurs at $\Phi = 1.56$, $\Phi = 1.57$, and $\Phi = 1.61$, respectively under these three Re_{air}. Under all these conditions, the tips of the inner reaction zone are open when $\Phi \leqslant 1.0$.

The heat flux distributions when the post-flame zone impinges on the plate under different ϕ are shown in Fig. 9e. The variation trend is similar to that under reaction cone tip impingement, except that only one peak heat flux point appears which locates at the stagnation point. This corresponds to the fact the maximum flame temperature and the maximum impinging velocity occur at the stagnation point. Thus, all the curves are bell-shaped.

The heat flux distributions under small H/d_{air} of 3.0 when the cold unreacted gas inside the reaction cone impinges on the plate are illustrated from Figs. 9f–9h, respectively. It is observed that under all the three Re_{air}, the variation trend is similar to each other, with an extremely low heat flux around the stagnation point around or below zero and two apexes some radial distance away. It is observed that the values of the heat flux at the stagnation point are the same despite increasing ϕ from the fuel-lean condition to the fuel-rich condition under all the experimental conditions, except the far lower level occurred when $Re_{air} = 8000$, $\Phi = 0.8$. Also except this condition, the heat flux increases from the stagnation point to the maximum value point following almost a same line when increasing ϕ. Beyond the maximum heat flux location, the local heat flux starts to decrease monotonically, with higher value coming under larger ϕ. This is due to the increased flame length under larger ϕ. It is also observed from Figs. 9f–9h that as increasing ϕ, the maximum heat flux increases gradually till $\Phi = 1.4$ and no clear increase is found beyond that. On the other hand, the location of the maximum heat flux turns further outwards all the way.

5.3. Effects of Re_{air}

The influences of the Re_{air} on the local heat transfer rate is illustrated in Fig. 10. Re_{air} varies from 3000 to 8000, while the values of the ϕ is selected to be 1.0 and 1.4, and the H/d_{air} to be 3 and 9, respectively.

The comparisons of the heat flux distributions under smaller H/d_{air} of 3.0 when $\Phi = 1.0$ and $\Phi = 1.4$, are shown in Figs. 10a and 10b, respectively. It is observed that under all conditions, the heat flux varies following a similar trend line, with an extremely low level of heat flux around the stagnation point and two heat flux apexes located some distance away. The maximum heat flux increases with the increase in Re_{air}. Generally, the location of the maximum heat flux is shifted further away radially under larger Re_{air}. The heat flux beyond the apex increases with the increase in

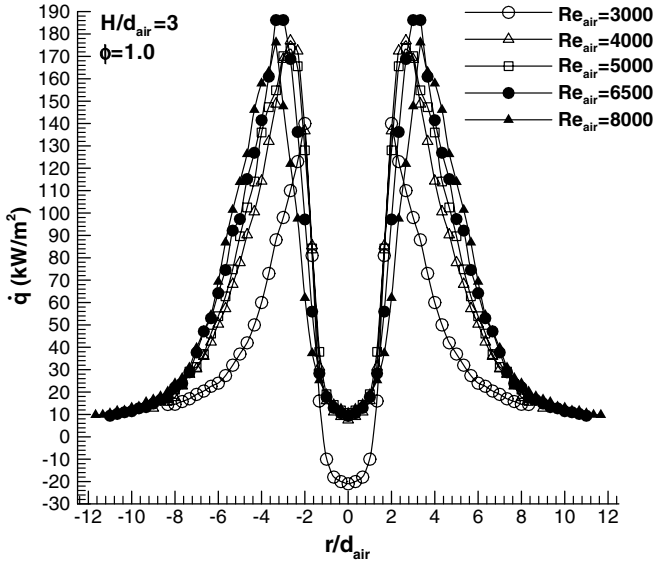

Fig. 10a. Variations of heat flux with Re_{air} under $\Phi = 1.0$, $H/d_{air} = 3$.

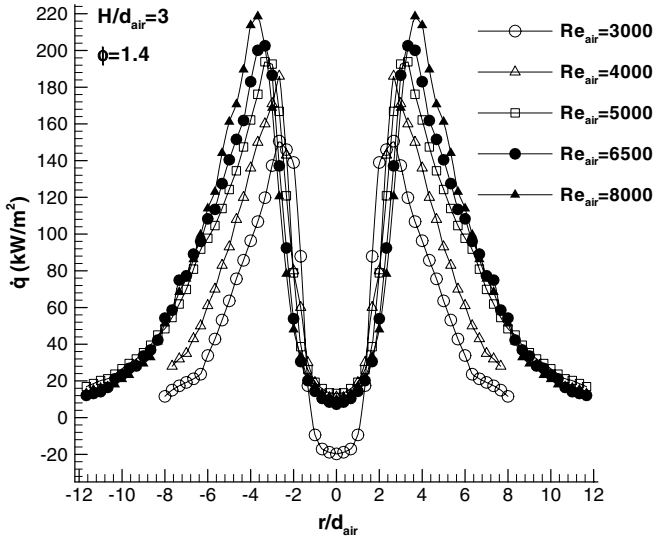

Fig. 10b. Variations of heat flux with Re_{air} under $\Phi = 1.4$, $H/d_{air} = 3$.

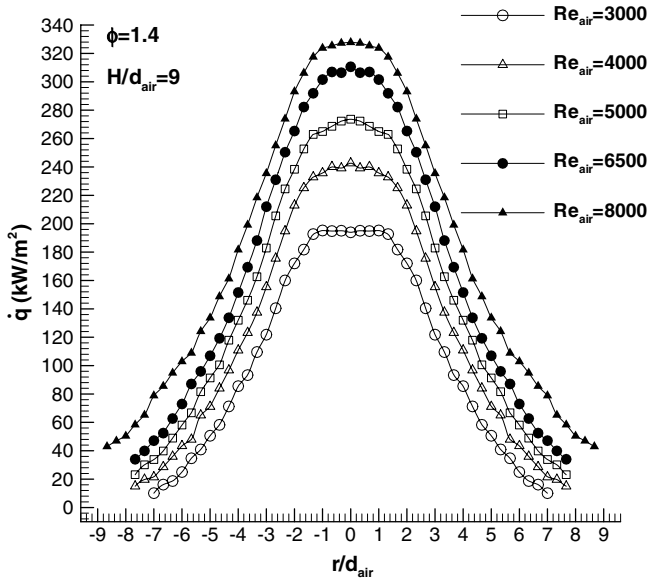

Fig. 10c. Variations of heat flux with Re_{air} under $\Phi = 1.4$, $H/d_{air} = 9$.

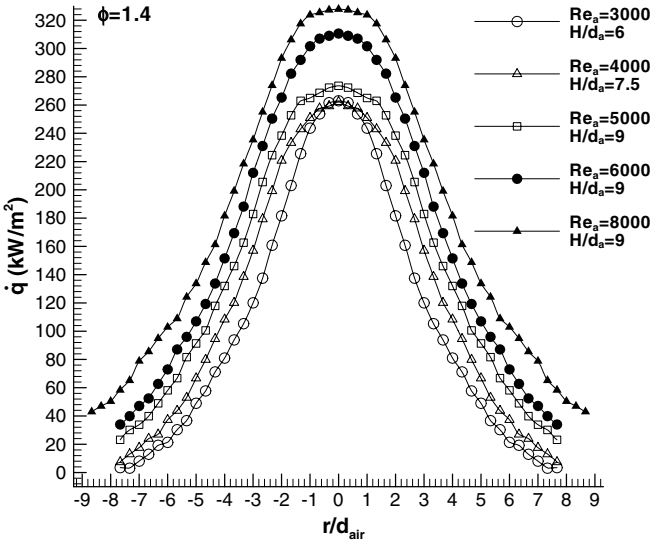

Fig. 10d. Variations of maximum heat flux with Re_{air} under $\Phi = 1.4$.

Re_{air}, till approximately $r/d_{air} = 8.0$, where the difference between them is indistinguishable. The heat flux distribution under $H/d_{air} = 9$ is illustrated in Fig. 10c. It is observed that the heat flux variation trend line is of bell-shape under all the conditions. The heat flux increases monotonically with increasing the Re_{air}. This is due to the combined effect of the flame temperature, turbulence and the chemical reaction heat release. As we have discussed before, the flame length including the inner cone and the outer layer increases with the increase in the Re_{air}. When $Re_{air} \leqslant 5000$, it is the post-flame zone that impinges on the plate, while the tip of the inner reaction zone impinges on the plate in the other two conditions. The enhanced flame temperature, enhanced turbulence and the occurrence of the chemical reaction all contribute to

the heat transfer enhancement under larger Re_{air}. Fig. 10d compares the maximum heat fluxes achieved under different Re_{air}. Under all the conditions, the tip of the inner reaction zone impinges on the plate. It is observed that the stagnation point heat fluxes are similar in value under $Re_{air} = 3000$ and $Re_{air} = 4000$. A noticeable increase is only observed when $Re_{air} \geqslant 5000$. On the other hand, in the region beyond the stagnation point, the local heat flux increases steadily with the increase in Re_{air}. It can also be observed from Fig. 10d that as increasing the Re_{air}, the heat flux distribution around the stagnation point becomes flatter. This is the result the increased thickness of the inner reaction cone tip under higher Re_{air}, as discussed before.

6. Averaged heat transfer characteristics

To better understand the thermal performance of the impinging IDF, the averaged heat flux distributions under varied parameters are presented in Fig. 11. The averaged heat flux is obtained by integrating the local heat flux with the trapezoid rule. The integration area is $0 \leqslant r/d_{air} \leqslant 7.0$, which comprises the impingement zone and the wall jet zone where the local heat flux generally is over 20 kW/m^2.

The dependency of the averaged heat flux, i.e., $\bar{q}$, on H/d_{air}, is illustrated in Fig. 11a. It is observed that under the same ϕ of 1.4, the $\bar{q}$ increases monotonically with the increase in Re_{air}. The variation trend with the H/d_{air} is similar to each other under each Re_{air}. First, the $\bar{q}$ increases rapidly and almost linearly from $H/d_{air} = 3$ to the peak value. Then it decreases gradually as further increasing the H/d_{air} at a slower pace, but also following a linear trend line. In the selected integration region, the maximum $\bar{q}$ is obtained when $H/d_{air} = 6$ for $Re_{air} = 3000$ and $Re_{air} = 4000$. The maximum $\bar{q}$ occurs under $H/d_{air} = 7$ and $H/d_{air} = 9$ for $Re_{air} = 5000$ and $Re_{air} = 6500$, respectively. When the Re_{air} increases to 8000 and the ϕ increases

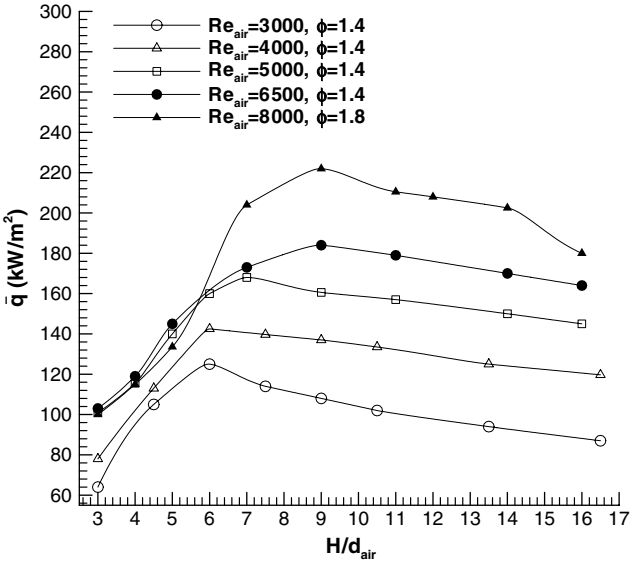

Fig. 11a. Variations of average heat flux with H/d_{air}.

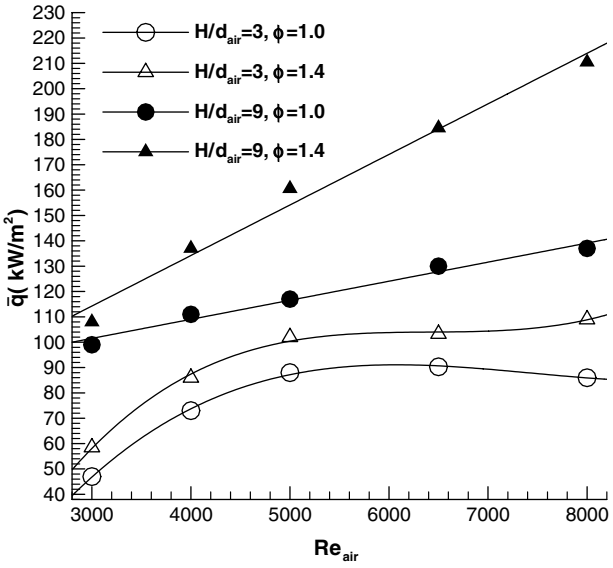

Fig. 11b. Variations of average heat flux with Re_{air}.

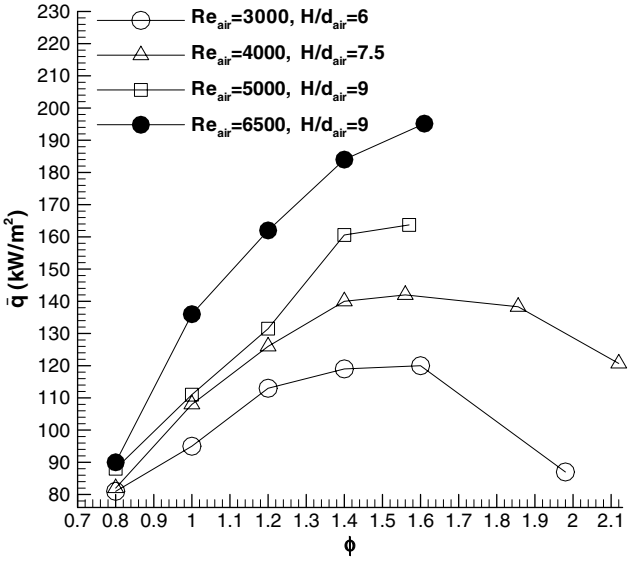

Fig. 11c. Variations of average heat flux with Φ.

to 1.8, it is observed that the $\bar{q}$ is slightly lower than that under $Re_{air} = 5000$, $\Phi = 1.4$. This is the result of the reduced flame temperature associated with incomplete combustion under larger ϕ despite the turbulence-augmentation effect. When H/d_{air} reaches 7.0 and beyond, the $\bar{q}$ comes the highest in the chart, with the peak value occurs under $H/d_{air} = 9$. Beyond that, the $\bar{q}$ decreases gradually, as the other cases under $\Phi = 1.4$.

The variation of the $\bar{q}$ with the Re_{air} is shown in Fig. 11b. Two H/d_{air} are selected to be 3.0 and 9.0. The values of the selected ϕ are 1.0 and 1.4. It is observed that the $\bar{q}$ increases steadily with the increase in the Re_{air} under these four conditions. Specifically, under small H/d_{air} of 3.0, the $\bar{q}$ increases fast from $Re_{air} = 3000$ to $Re_{air} = 5000$ under both conditions of $\Phi = 1.0$ and $\Phi = 1.4$. Beyond

that, only a slight increase is found when further increasing the Re_{air} to 8000 under $\Phi = 1.4$. As a contrast, the $\bar{q}$ keeps little changed when increasing the Re_{air} from 5000 to 6500 under $\Phi = 1.0$. Then a slight decrease is observed when further increasing the Re_{air} to 8000. The reduced heat flux is due to the reduced flame temperature under higher Re_{air} where more air is entrained, resulting in a actual fuel-lean condition although the initial ϕ is set to 1.0. On the whole, both the $\bar{q}$ under these two conditions vary following a respective polynomial curve. By comparison, the $\bar{q}$ increases linearly under $H/d_{air} = 9.0$, with a faster pace under $\Phi = 1.4$.

The variations of the $\bar{q}$ with the ϕ are shown in Fig. 11c. It is observed that under all the Re_{air}, the $\bar{q}$ under $\Phi = 0.8$ are similar to each other, with only a slightly increase with the increase in the Re_{air}. This is due to the fuel-lean conditions under all the Re_{air} lowering the flame temperature, and thus the local heat flux, as discussed before. Beyond that, the $\bar{q}$ increases gradually till a peak value occurred around $\Phi = 1.6$. The larger the Re_{air}, the faster the pace. Further increase in the ϕ leads to soot emission, as discussed in the above, which results in the decrease in the local heat flux, and also the average heat flux, as shown in Fig. 11c.

7. Comparison of the heat transfer rate with premixed flame jet

To evaluate the thermal performance of this blue impinging IDF, comparisons of the heat transfer rate are made with those in premixed flame jet (PFJ) by Dong et al. [23], as shown in Fig. 12. The diameter of the inner burner tube used in Dong et al. [23] is 10 mm, while the air port diameter is 6 mm in the present IDF burner. Other than this, the other parameters, including ϕ, Reynolds number and the non-dimensional burner/plate distance, are kept the same to each other. It is observed in Fig. 12 that on the whole, the heat transfer rates from both the flames are in the similar level. The $\dot{q}_{max}$ is around 190 kW/ m^2 in both the cases, and occurs at the location around r/d(or d_{air}) = 1.0. However, in the impingement region and the early wall jet region of r/d(or d_{air}) < 4.0, the $\dot{q}$ from the IDF come higher than those form the PFJ except the $\dot{q}_{max}$. Beyond it, the $\dot{q}$ from the IDF are a little lower than those from the PFJ. Thus, in the whole region, the IDF gives a little higher averaged heat flux than that produced by the PFJ. On the other hand, due to the difference in the burner diameter, less fuel is consumed in the IDF than the PFJ under the same ϕ, Reynolds number and the non-dimensional burner/plate distance. The fuel consumption in the IDF is only 60% of that in the PFJ, which is proportional to the ratio of (d_{air}/d). Therefore, it is clear that the IDF could produce higher heat flux than the PFJ with the fuel consumption 40% less than the PFJ. It is believed that this heat transfer enhancement is due to the enhanced turbulence level in the IDF. Strong mixing of fuel and air occurs in the flame neck, originating extra turbulence in addition to the initial turbulence in the free stream, thus enhancing the heat transfer rate.

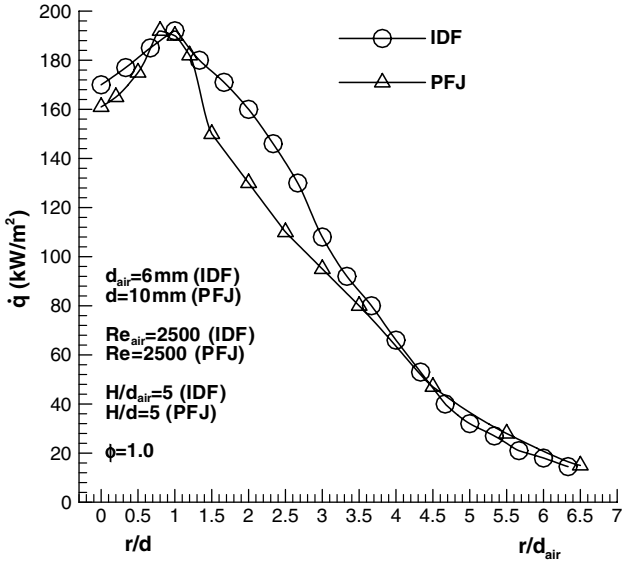

Fig. 12. Comparison of $\dot{q}$ between IDF and PFJ.

8. Conclusions

Having identified the blue, dual-structured, triple-layered IDF as the favorable flame jet for impingement heating in the first part of this paper, this part is the continuation to the first one. The flame structure, static wall pressure characteristics, and local and averaged heat transfer characteristics of this type of blue impinging inverse diffusion flames have been investigated experimentally. The following conclusions can be drawn:

1. Four types of impinging IDF are identified. By increasing the H/d_{air} gradually, the flame structure can vary from the impingement of the cold gas inside the inner reaction zone, to the impingement of the tip of the reaction zone, and finally to the impingement of the post-flame zone. The fourth flame structure is formed when ϕ is as small as 0.8, where the tip of the inner reaction zone is open before impingement. Increase in ϕ and Re_{air} increases the whole flame length and the length of the inner cone tip. A yellow neck and/or yellow flame tip appear under lower Re_{air} of 3000 and 4000 under $H/d_{air} = 9$, $\Phi = 1.4$, due to the soot emission associated with incomplete combustion under insufficient fuel/air mixing.
2. The stagnation point wall pressure remains constant when the potential core region impinges on the plate. The P_s starts to decrease as increasing H/d_{air} due to reduced impinging velocity. The P_s remains at a low level under large H/d_{air} of over around 11 due to the much weakened influence of the jet exit velocity. Under the condition of $Re_{air} = 4000$, $\Phi = 1.4$, the length of the impingement region increases first from $r/d_{air} = 1.8$ to

$r/d_{air} = 4.2$ with increasing H/d_{air} from 1.5 to 7.5. Then it decreases to $r/d_{air} = 1.7$ with further increasing in H/d_{air} to 16.5. As increasing ϕ, the P_s decreases monotonically and the pressure gradient increases gradually. Under the condition of $Re_{air} = 6400$, $H/d_{air} = 9$, the impingement region increases generally with increase in ϕ ranging from $r/d_{air} = 2.7$ under $\Phi = 0.8$ to $r/d_{air} = 3.5$ under $\Phi = 1.61$.

3. Heat flux increases with increasing H/d_{air} at first until the maximum value achieved when the inner reaction cone tip impinges directly on the plate. After that, the heat flux decreases gradually with further increasing H/d_{air} till $H/d_{air} = 10$ although T_f remains almost unchanged. This decrease in heat flux is due to the decrease in the impinging velocity. When $H/d_{air} > 10$, the heat flux distribution remains little changed due to small impinging velocity and relatively constant flame temperature until $H/d_{air} = 20$. Under $\Phi = 1.4$, the $\bar{q}$ increases linearly from $H/d_{air} = 3.0$ to a peak value. Then a slower linear decrease in $\bar{q}$ is followed when further increasing H/d_{air}. This variation trends are similar to each other under different Re_{air}.
4. When ϕ varies from fuel-lean condition to fuel-rich condition where the reaction cone tip impinges on the plate, the maximum heat flux increases accordingly and its location shifts gradually inwards till reaching the stagnation point. The cold impingement plate quenches the flame and causes the tip of the IDF to open under larger ϕ than that in the free flame. When yellow-tip flame appears under higher ϕ, the maximum heat flux decreased dramatically due to reduced flame temperature associated with incomplete combustion. In the wall jet region, higher heat transfer is achieved under larger equivalence ratio due to prolonged flame length and thus extended area in the plate that contacts the flame. The averaged heat flux increases steadily with the increase in the ϕ to a peak value at around $\phi = 1.6$. Then it decreases gradually with further increase in ϕ.
5. Impinging IDF is found to produce higher heat transfer rate than the premixed flame jet due to the augmented turbulence level created by the strong mixing of fuel and air in the flame neck.

Acknowledgement

The authors wish to thank The Hong Kong Polytechnic University and the Research Grants Council of the Hong Kong SAR (Project No. PolyU 5142/05E) for financial support of the present study.

References

[1] G.K. Hargrave, M. Fairweather, J.K. Kilham, Forced convective heat transfer from premixed flames – part 1: flame structure, Int. J. Heat Fluid Flow 8 (1) (1987) 55–63.

[2] J.M. Beer, N.A. Chigier, Impinging jet flames, Combust. Flame 12 (1968) 575–586.

[3] J.W. Mohr, J. Seyed-Yagoobi, R.H. Page, Heat transfer characteristics of a radial jet reattachment flame, J. Heat Transfer 119 (1997) 258–264.

[4] M.E. Horsley, M.R.I. Purvis, A.S. Tariq, Convective heat transfer from laminar and turbulent premixed flames, Heat Transfer (3) (1982) 409–415.

[5] R. Rigey, B.W. Webb, An experimental investigation of diffusion flame jet impingement heat transfer, in: Proceedings of the ASME/JSME Thermal Engineering Joint Conference, vol. 3, 1995, pp. 117–126.

[6] A. Milson, N.A. Chigier, Studies of methane and methane–air flames impinging on a cold plate, Combust. Flame 21 (1973) 295–305.

[7] C.E. Baukal, L.K. Farmer, B. Gebhart, I. Chan, Heat transfer mechanisms in flame impingement heating, in: Proceedings of the 1995 International Gas Research Conference, vol. 2, 1996, pp. 2277–2287.

[8] C.E. Baukal, B. Gebhart, Surface condition effects on flame impingement heat transfer, Exp. Thermal Fluid Sci. 15 (1997) 323–335.

[9] C.E. Baukal, B. Gebhart, Heat transfer from oxygen-enhanced/natural gas flames impinging normal to a plane surface, Exp. Thermal Fluid Sci. 16 (1998) 247–259.

[10] C.J. Hoogendoorn, Cz.O. Popiel, Th.H. van der Meer, Turbulent heat transfer on a plane surface in impingement round premixed plate jets, Int. Heat Transfer Conference, 1978, pp. 107–112.

[11] E. Buhr, G. Haupt and H. Kremer, Heat Transfer from Impinging Turbulent Jet Flames to Plane Surfaces, Combustion Institute European Symposium 1973E, 1973.

[12] J.W. Mohr, J. Seyed-Yagoobi, R.H. Page, Combustion measurements from an impinging radial jet reattachment flame, Combust. Flame 106 (1996) 69–80.

[13] L.L. Dong, C.W. Leung, C.S. Cheung, Combustion optimization of a slot flame jet impinging system, J. Inst. Energy 76 (2003) 80–88.

[14] J.W. Mohr, J. Seyed-Yagobi, R.H. Page, Optimization of a practical radial jet reattachment flame, National Heat Transfer Conference, vol. 2, 1995, pp. 3–10.

[15] J.W. Mohr, J. Seyed-Yagobi, R.H. Page, Combustion measurements from an impinging radial jet reattachment flame, Combust. Flame 106 (1996) 69–80.

[16] G.K. Hargrave, J.K. Kilham, The effect of turbulence intensity on convective heat transfer from premixed methane–air flames, Institute of Chemical Engineering Symposium Series, vol. 2, 1984, pp. 1025–1034.

[17] G.K. Hargrave, M. Fairweather, J.K. Kilham, Forced convective heat transfer from premixed flames – part 2: impingement heat transfer, Int. J. Heat Fluid Flow 8 (2) (1987) 132–138.

[18] H. Kremer, E. Buhr, R. Haupt, Heat Transfer from Turbulent Free-Jet Flames to Plate Surfaces, 1973, pp. 463–472.

[19] J.E . Anderson, E.F. Stresino, Heat transfer from flames impinging on flat and cylindrical surfaces, J. Heat Transfer 85 (1963) 49–54.

[20] M. Fairweather, J.K. Kilham, A. Mohebi-Ashtiani, Stagnation point heat transfer from turbulent methane–air flames, Combust. Sci. Technol. 35 (1985) 225–238.

[21] S.G. Tuttle, B.W. Webb, M.Q. Mcquay, Convective heat transfer from a partially premixed impinging flame jet. Part 1: time-averaged results, Int. J. Heat Mass Transfer 48 (7) (2005) 1236–1251.

[22] S.J. Kline, F.A. McClintock, Describing uncertainties in single sample experiments, Mech. Eng. 75 (1953) 3–8.

[23] L.L. Dong, C.S. Cheung, C.W. Leung, Heat transfer characteristics of an impinging butane/air flame jet of low Reynolds number, Exp. Heat Transfer 14 (2001) 265–282.